Geotextiles and Geomembranes 53 (2025) 1687–1698

Contents lists available at ScienceDirect

Geotextiles and Geomembranes

journal homepage: www.elsevier.com/locate/geotexmem

Regular paper

A simple 3D orthotropic model for the tensile response of geogrids: In-isolation and soil–geogrid interaction applications

Lucas Paiva [a,*], Margarida Pinho-Lopes [a], Robertt Valente [b], António Miguel Paula [c]

[a] CERIS, Department of Civil Engineering, University of Aveiro, Campus Universitário de Santiago, Aveiro, 3810-193, Portugal
[b] TEMA, Department of Mechanical Engineering, University of Aveiro, Campus Universitário de Santiago, Aveiro, 3810-193, Portugal
[c] GiCos, Instituto Politécnico de Bragança, Campus de Santa Apolónia, 5300-253 Bragança, Portugal

ARTICLE INFO

Dataset link: https://github.com/luccpaiva/ortho-model

Keywords:
Geogrids
ABAQUS
Numerical modelling
Plasticity
Orthotropy
Damage

ABSTRACT

The short-term tensile response is one of the key aspects in designing geogrid-reinforced soil structures. In this paper a simple data-driven 3D orthotropic model for the short-term tensile response is proposed. The Hill48 yield model is chosen to represent the orthotropic behaviour of the geogrid, and a procedure to obtain the necessary parameters, from simple tensile test data, is presented. The model is then implemented in ABAQUS, and validated against a realistic problem where the geogrid is embedded in soil. The influence of the orthotropy (against isotropy) on both the reinforcement and the overall soil–geogrid structure is evaluated. The results show that the orthotropic model can accurately predict the tensile response of the geogrid in different directions, with the orthotropy having a significant influence on the reinforcement and the overall structural response, especially in highly orthotropic materials. The study further examined stress redistribution capabilities in geogrids with notches, revealing enhanced stabilization performance using the orthotropic model. Parametric tests indicated that traditional isotropic assumptions might underpredict or overpredict reinforcement performance, emphasizing the advantages for accurate orthotropic characterization. The proposed 3D framework provides a robust, straightforward method for evaluating and optimizing geogrid designs, enabling better prediction of reinforced soil behaviour in geotechnical applications.

1. Introduction

Numerical modelling, for example using the Finite Element Method (FEM), has been widely used to study the mechanical behaviour of geosynthetics, both in isolation and embedded in soil. The advantages of such method include the possibility of accounting for complex geometrical and boundary conditions and soil–geosynthetic interaction, besides including nonlinear material models that closely replicate the actual response of geosynthetic-reinforced structures. However, gathering experimental data to calibrate these models is often challenging, as the number of parameters required to precisely define boundary conditions and material properties can be extensive, some requiring complex testing procedures or even trial and error approaches. Because of this complexity, simplifications are often made when using FEM, on geometry, material properties and contact conditions.

Geogrids, a particular type of geosynthetic, are used primarily for soil reinforcement. A geogrid consists of a planar, polymeric structure with a grid-like configuration, characterized by tensile members that form a regular network of ribs and junctions. These structures are designed to interlock with the surrounding soil, creating a composite behaviour that enhances the strength and stability of the soil–geosynthetic system. Geogrids can be manufactured from various polymers, such as polypropylene, polyester, or high-density polyethylene, and their mechanical significantly properties depend on both the material composition and the manufacturing process (Shukla, 2006).

Due to the polymeric composition and the manufacturing process, geogrids are often orthotropic materials, with different tensile properties in the machine direction (MD) and cross-machine directions (XMD) (Perkins, 2000). However, the exact influence of this orthotropy on the overall response of a soil–geogrid system is complex to determine, as it does not only depend on the geogrid properties, but also on soil properties, the geometry of the system and the boundary conditions. Early experimental investigations reported by Zhang et al. (2006) suggested that the anisotropic response of the reinforced soil increases with the number of layers of reinforcement, and the stiffness of the reinforcement. More recent studies (Gajewski and Jemioło, 2014) shown that geogrid modelling is often oversimplified, and the orthotropic effects can have a pronounced influence on the tensile response of the reinforcement. Zhuang and Wang (2015) performed parametric tests on a piled embankment, modelling the geogrid with

* Corresponding author.
E-mail addresses: lucaspaiva@ua.pt (L. Paiva), mlopes@ua.pt (M. Pinho-Lopes), robertt@ua.pt (R. Valente), mpaula@ipb.pt (A.M. Paula).

https://doi.org/10.1016/j.geotexmem.2025.07.010
Received 2 April 2025; Received in revised form 4 July 2025; Accepted 20 July 2025
Available online 29 August 2025

an orthotropic membrane and an isotropic membrane. Results in terms of vertical settlement were slightly higher (about 5 %) for the isotropic model, whereas yield stresses in the geogrid being overpredicted on the isotropic case by an average of 33 %.

The modelling aspect of orthotropy and its respective numerical implementation is therefore still a challenge. Geogrids, like many other polymeric materials, exhibit a combination of elastic, plastic and viscous responses when subjected to different loading conditions (Shukla, 2006). Moreover, even at low strain levels, geogrids often exhibit nonlinear plastic responses due to both manufacturing (e.g., the extrusion process creates structural anisotropy by preferentially aligning polymer chains in the machine direction (Al-Barqawi et al., 2021)) and material composition factors (e.g., viscoelastic nature of polymer matrix (Koerner, 2012; Ezzein et al., 2015)). One of the first two-dimensional orthotropic models proposed by Perkins (2000) required a total of 24 input parameters to fully characterize orthotropy (although not only for the short-term tensile response), an extensive set of tests being required to obtain the necessary data to fetch the constitutive law. Gajewski and Jemioło (2014) proposed a different approach, with fewer parameters from the experimental data, but the model was still complex in terms of geometry (dependent on fibre distribution) and only accounted for the elastic response of the geogrid. A simple orthotropic model, using the tangential stiffness on the MD and XMD directions was used by Huang et al. (2020), again limited to an elastic response of the geogrid, with the failure criterion being manually adopted as a limit strain value.

Given the complexity and/or extensive testing requirements of existing orthotropic models, there is a need for a simpler approach that can be more easily implemented in numerical models, while still capturing the essential orthotropic response with reasonable accuracy.

Focusing on these modelling aspects, the purpose of this paper is to present a simple 3D orthotropic modelling approach for the short-term tensile response of geogrids. Herein this is an immediate mechanical response under loading, validated against short-term tensile tests data typically with a loading rate of $20\,\mathrm{mm\,min^{-1}}$, according to ISO and ASTM testing standards (ISO-10319, 2015; ASTM-D6637-10, 2011). The model should be capable of being defined by standard tensile test data typically provided by geosynthetic manufacturers or obtained experimentally. This is done in two phases:

(I) to define a 3D nonlinear elastoplastic FEM-based approach for the tensile response of geogrids, with an orthotropic constitutive model that can be calibrated using standard tensile test data;
(II) to validate the model against a realistic problem where the geogrid is embedded in soil, evaluating the influence of the orthotropy (against isotropy) on both the reinforcement and the overall structural responses.

2. A data-driven orthotropic model for geogrids

This section details the theory behind the proposed orthotropic model and the procedure to obtain the relevant parameters from standard tensile test data.

2.1. A review of the Hill48 yield criterion

In plasticity mechanics, the yield function is a mathematical expression that determines the condition under which a material begins to deform plastically. The von Mises yield function is the most used yield criterion due to its good correlation with experimental data and relatively simple implementation in numerical models (Dunne and Petrinic, 2005). The von Mises yield function can be expressed in terms of normal σ and shear τ components as

$$f(\sigma) = \frac{1}{2}\left[(\sigma_{xx}-\sigma_{yy})^2+(\sigma_{yy}-\sigma_{zz})^2+(\sigma_{zz}-\sigma_{xx})^2+6(\tau_{xy}^2+\tau_{xz}^2+\tau_{yz}^2)\right]=\bar{\sigma}^2, \tag{1}$$

where x, y, z are the orthotropic directions for the stress components, and $\bar{\sigma}$ is the equivalent yield stress (a scalar quantity). The von Mises yield function does not account for the anisotropic nature of the material, since the yielding condition $f(\sigma)=\bar{\sigma}^2$ in Eq. (1) implies that the yielding is solely a function of the magnitude of the stress components and not their directional arrangement.

Among the generalizations to allow for an anisotropic behaviour, the Hill criterion (Hill, 1948) serves as an extension to the von Mises yield function, accounting for an anisotropic response of the material. This criterion, often designed as Hill48, can be written as

$$f(\sigma) = F(\sigma_{yy}-\sigma_{zz})^2+G(\sigma_{zz}-\sigma_{xx})^2+H(\sigma_{xx}-\sigma_{yy})^2+2L\tau_{yz}^2+2M\tau_{xz}^2+2N\tau_{xy}^2=\bar{\sigma}^2, \tag{2}$$

where F, G, H, L, M, N are material constants that define the anisotropic response of the material. When $F=G=H=3L=3M=3N$, Eq. (2) reduces to the von Mises yield function. The Hill48 yield function is a popular choice for modelling anisotropy because the material constants can be determined by yield stress ratios, thus making it easier to calibrate the criterion with experimental data (Wu and H.C, 2002). The Hill48 model was selected due to its practical advantages: calibration requires only uniaxial tensile tests in principal directions, unlike other models (e.g., Yld2000-2D, BBC2005) that demand more complex multiaxial testing (Wang et al., 2009; Khalfallah et al., 2015); and generally available in commercial FEM software without requiring user-defined subroutines.

Several studies have shown that the Hill48 model can capture the anisotropic response of many materials, including metal sheets (Haddadi et al., 2006; Zhu et al., 2014; Bruschi et al., 2014) and wood (Akter et al., 2021). However, the simplicity of the Hill48 model also comes with limitations. Notably, the inability to capture the anisotropic response of materials with strong anisotropy and the definition of anisotropic coefficients that could either predict the stress ratios (i.e., the yield stresses in different directions) or the directional flow stress (related to initiation/continuation of plastic deformations), but not both simultaneously (Barlat et al., 1991; Hill, 1993; Cardoso and Adetoro, 2018; Mu et al., 2022). Although the Hill48 model is proven to be a good approximation to many cases of anisotropy for a variety of materials, a robust framework is needed to correctly determine the anisotropic coefficients and verify its applicability to present specific case of geogrids. The next sections are dedicated to the calibration of the Hill48 model for geogrids, and the numerical implementation of the model in ABAQUS (Abaqus, 2021).

2.2. Uniaxial tensile yield stress

The goal of this section is to establish a procedure to evaluate the orthotropic parameters of the Hill48 model using standard tensile test data. Initially, a stress at a given angle is written in terms of a ratio between a reference stress value. After, a procedure is defined to determine the Hill48 parameters using the stress ratios.

On the function of reinforcement, the stresses acting on the perpendicular plan of the geogrid are usually ignored. Then, in Eq. (2), the terms related to the shear stresses are neglected, and the yield function can be simplified to

$$f(\sigma) = (G+H)\sigma_{xx}^2-2H\sigma_{xx}\sigma_{yy}+(H+F)\sigma_{yy}^2+2N\tau_{xy}^2=\bar{\sigma}^2. \tag{3}$$

Although the yield function in Eq. (3) can be used in FEM simulations with both shell-type and solid-type elements (for the 3D case), only stresses along the normal directions of the element should be considered. Then, it is necessary to define the relevant stress directions. Taking the MD direction as the x-axis, and the perpendicular direction (XMD) as the y-axis, the yield stress in the MD direction can be set as the reference stress, written as

$$\sigma_{xx}=\sigma_0=\bar{\sigma}. \tag{4}$$

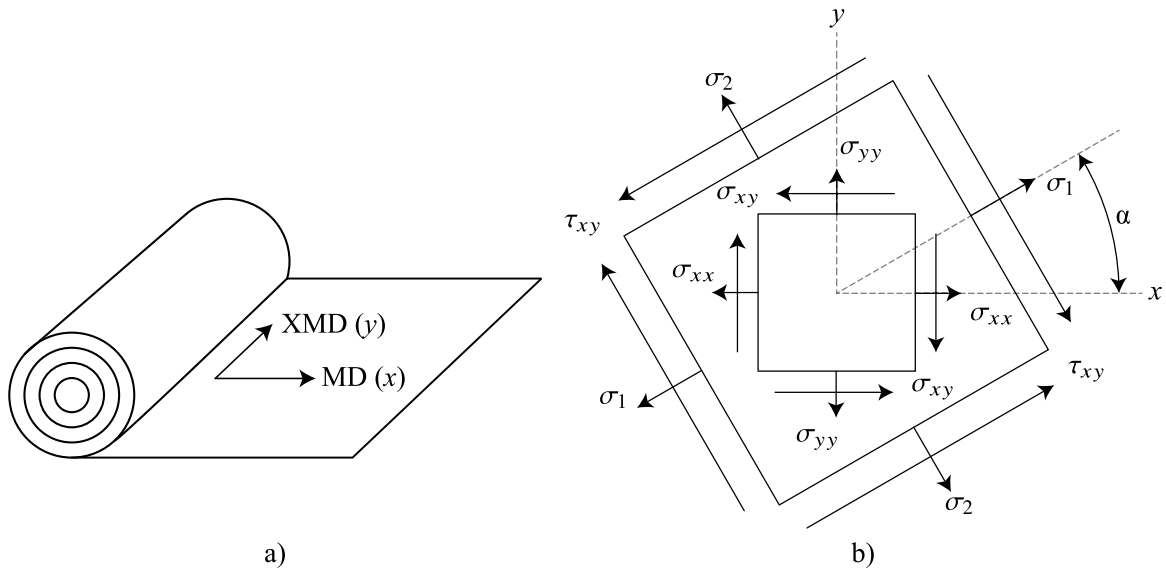

Fig. 1. Stresses and corresponding directions at an angle α with respect to the MD and XMD directions.

Using the stress transformation equations, the following relations are established:

$$\sigma_x = \sigma_1 \cos^2\alpha + \sigma_2 \sin^2\alpha - 2\tau_{xy}\cos\alpha\sin\alpha, \tag{5a}$$

$$\sigma_y = \sigma_1 \sin^2\alpha + \sigma_2 \cos^2\alpha + 2\tau_{xy}\cos\alpha\sin\alpha, \tag{5b}$$

$$\sigma_{xy} = (\sigma_1 - \sigma_2)\cos\alpha\sin\alpha + \tau_{xy}(\cos^2\alpha - \sin^2\alpha), \tag{5c}$$

where σ_1 is the stress along the direction of an angle α with respect to the reference direction, σ_2 is the stress perpendicular to σ_1, and τ_{xy} is the shear stress acting on the plane. A representation of the reference directions and this transformation is shown in Fig. 1.

The reference stress angle $\alpha = 0°$, taken as the rolling MD direction, is set to be α_0. In this reference direction, $\sigma_1 = \sigma_0$ and $\sigma_2 = \tau_{xy} = 0$. Thus, Eq. (5) becomes

$$\sigma_{xx} = \alpha_\alpha \cos^2\alpha, \tag{6a}$$

$$\sigma_{yy} = \alpha_\alpha \sin^2\alpha, \tag{6b}$$

$$\sigma_{xy} = \alpha_\alpha \sin\alpha\cos\alpha. \tag{6c}$$

The uniaxial tensile yield stress at an arbitrary angle α with respect to the reference direction, combining Eq. (3), (4) and (6), can be written as

$$\sigma_\alpha = \frac{\sigma_0}{\sqrt{(G+H)\cos^4\alpha + (F+H)\sin^4\alpha + 2(N-H)\sin^2\alpha\cos^2\alpha}}. \tag{7}$$

2.3. Associated plastic potential

The yield stress defined by Eq. (7) can be used to determine the plastic potential. Given the plastic increments $d\varepsilon_x$, $d\varepsilon_y$, $d\gamma_{xy}$, and a proportionality factor $d\lambda$, the flow can be obtained according to Hill stability criterion (Hill, 1958):

$$d\varepsilon_{xx} = d\lambda\left[2(G+H)\sigma_{xx} - 2H\sigma_{yy}\right], \tag{8a}$$

$$d\varepsilon_{yy} = d\lambda\left[2(F+H)\sigma_{yy} - 2H\sigma_{xx}\right], \tag{8b}$$

$$d\gamma_{xy} = 4d\lambda N\tau_{xy}. \tag{8c}$$

When the stresses are expressed in terms of an angle α, the plastic strains are written as follows, combining Eq. (6) and (8):

$$d\varepsilon_{xx} = d\lambda\left[2(G+H)\sigma_\alpha\cos^2\alpha - 2H\sigma_\alpha\sin^2\alpha\right], \tag{9a}$$

$$d\varepsilon_{yy} = d\lambda\left[2(F+H)\sigma_\alpha\sin^2\alpha - 2H\sigma_\alpha\cos^2\alpha\right], \tag{9b}$$

$$d\gamma_{xy} = 4d\lambda N\sigma_\alpha\sin\alpha\cos\alpha. \tag{9c}$$

A relationship between the strain directions, according to the Mohr's circle, can be written as

$$\varepsilon_\alpha = \frac{\varepsilon_x + \varepsilon_y}{2} + \frac{\varepsilon_x - \varepsilon_y}{2}\cos 2\alpha + \frac{\gamma_{xy}}{2}\sin 2\alpha. \tag{10}$$

The strains obtained for an arbitrary angle α can then be used to describe the potential ratios. The relation between the strain increments in the loading direction, $d\varepsilon_\alpha$, and in the perpendicular direction, $d\varepsilon_{\alpha+\pi/2}$, can be written as

$$d\varepsilon_\alpha = d\varepsilon_{xx}\cos^2\alpha + d\varepsilon_{yy}\sin^2\alpha + d\gamma_{xy}\sin\alpha\cos\alpha, \tag{11a}$$

$$d\varepsilon_{\alpha+\pi/2} = d\varepsilon_{xx}\sin^2\alpha + d\varepsilon_{yy}\cos^2\alpha - d\gamma_{xy}\sin\alpha\cos\alpha. \tag{11b}$$

Assuming a constant plastic volume, the infinitesimal strains are related by

$$d\varepsilon_x + d\varepsilon_y + d\varepsilon_z = 0, \tag{12a}$$

$$d\varepsilon_z = -(d\varepsilon_x + d\varepsilon_y) = -2\left(G\cos^2\alpha + F\sin^2\alpha\right)\sigma_\alpha d\lambda, \tag{12b}$$

and therefore the strain ratio, at an arbitrary angle α, can be written as

$$r_\alpha = \frac{d\varepsilon_{\alpha+\pi/2}}{d\varepsilon_z} = \frac{H + (2N - F - G - 4H)\sin^2\alpha\cos^2\alpha}{F\sin^2\alpha + G\cos^2\alpha}. \tag{13}$$

2.4. Hill48 parameters estimation using r-values

It is clear that $\alpha = 0°$ and $\alpha = 90°$ are two solutions of Eq. (13). The estimation of the anisotropy parameters for the Hill48 model can be done by evaluating the strain ratios at these two angles, with one additional angle being required. In the classical approach, the orthotropic parameters are usually defined using three experimental coefficients, r_0, r_{45} and r_{90}, which are then fed into Eq. (7) and (13) to derive the parameters algebraically. When both equations are satisfied, Hill48 model can predict the uniaxial yield stress at arbitrary directions with good accuracy (Lian et al., 2018). A more pragmatic approach is to use an r-value cost function (Neto et al., 2014), defined as

$$\text{cost}(F,G,H,N) = \sum\left(\frac{\sigma_\alpha}{\sigma_\alpha^{\exp}}\right)^2, \tag{14}$$

where σ_α^{exp} is the experimental yield stress at an angle α, and σ_α is the yield stress predicted by the Hill48 model, evaluated by Eq. (13). The parameters F, G, H, N are then adjusted to minimize the cost,

and the result of such minimization is the set of parameters that best describes the orthotropic response of the material. It is worth noting that, even though the experimental data in three directions would be sufficient to uniquely define the Hill48 parameters (as one of the directions can be set as reference), the cost function in Eq. (14) can lead to non-unique solutions due to multiple local minima and parameter correlation (Mu et al., 2022).

2.5. Numerical implementation in ABAQUS

The Hill48 model is implemented in ABAQUS through the definition of the yield stress ratios R_i (Abaqus, 2021). The following procedure is then used to convert the Hill48 parameters from Eq. (14) to the ABAQUS input parameters. For simplification purposes, the relevant equations will be simplified to the plane stress condition.

The yield stress ratios are defined with respect to a reference yield stress σ_0, such that if an arbitrary stress σ_{ij} is applied as the only nonzero stress, the corresponding yield stress is $R_{ij}\sigma_0$. In the uniaxial tensile test, only one stress component is non-zero at a time. Under this condition, a tensile test performed in the direction of σ_{11} would be expressed as

$$f(\sigma_{11}) = \sigma_0 \implies \sqrt{H\sigma_{11}^2} = \sigma_0 \implies H\sigma_{11}^2 = \sigma_0^2 \implies H = \frac{\sigma_0^2}{(\sigma_0 R_{11})^2} = \frac{1}{R_{11}^2}, \tag{15}$$

and similarly for the remaining directions:

$$f(\sigma_{22}) = \sigma_0 \implies F = \frac{\sigma_0^2}{(\sigma_0 R_{22})^2} = \frac{1}{R_{22}^2}, \tag{16a}$$

$$f(\sigma_{33}) = \sigma_0 \implies G = \frac{\sigma_0^2}{(\sigma_0 R_{33})^2} = \frac{1}{R_{33}^2}. \tag{16b}$$

Combining the results from the uniaxial tensile tests and taking into account the symmetry of the yield function, a relation between the Hill48 parameters and the yield ratios can be written as

$$F = \frac{1}{2}\left(\frac{1}{R_{22}^2} + \frac{1}{R_{33}^2} - \frac{1}{R_{11}^2}\right), \tag{17a}$$

$$G = \frac{1}{2}\left(\frac{1}{R_{33}^2} + \frac{1}{R_{11}^2} - \frac{1}{R_{22}^2}\right), \tag{17b}$$

$$H = \frac{1}{2}\left(\frac{1}{R_{11}^2} + \frac{1}{R_{22}^2} - \frac{1}{R_{33}^2}\right), \tag{17c}$$

$$N = \frac{3}{2}\left(\frac{\sigma_0}{\sigma_{12}}\right)^2 = \frac{3}{2}R_{12}^2. \tag{17d}$$

By solving Eq. (17) for the yield ratios, ABAQUS input values for the Hill48 orthotropic model can be written in terms of the orthotropic parameters:

$$R_{11} = \sqrt{\frac{1}{G+H}}, \tag{18a}$$

$$R_{22} = \sqrt{\frac{1}{F+H}}, \tag{18b}$$

$$R_{33} = \sqrt{\frac{1}{G+F}}, \tag{18c}$$

$$R_{12} = \sqrt{\frac{3}{2N}}. \tag{18d}$$

Given the form of the yield ratios, a well-defined yield function requires positive values for yield ratios. If one or more ratios are negative, the yield function may be undefined for a certain stress range, since the quantity under the square root is negative. It should be noted that, even for the orthotropic case, the ratios R_{13} and R_{23} must be provided in ABAQUS, and are equal to the unity.

Lastly, the flow rule is implemented in ABAQUS as

$$\mathrm{d}\epsilon^{pl} = \mathrm{d}\lambda \frac{\partial f}{\partial \boldsymbol{\sigma}} = \frac{\mathrm{d}\lambda}{f}\mathbf{b}, \tag{19}$$

where f is the Hill48 yield function, $\boldsymbol{\sigma}$ is the stress tensor, $\mathrm{d}\lambda$ is a plastic multiplier and $\mathbf{b}$ is the plastic potential gradient, defined as

$$\mathbf{b} = \begin{bmatrix} -G(\sigma_{33}-\sigma_{11}) + H(\sigma_{11}-\sigma_{22}) \\ F(\sigma_{22}-\sigma_{33}) - H(\sigma_{11}-\sigma_{22}) \\ -F(\sigma_{22}-\sigma_{33}) + G(\sigma_{33}-\sigma_{11}) \\ 2N\sigma_{12} \end{bmatrix}. \tag{20}$$

The plastic multiplier $\mathrm{d}\lambda$ is determined through the return mapping algorithm, ensuring that the stress state remains on the yield surface during plastic loading. Moreover, Eq. (19) implies that associated flow is defined, since the plastic potential is the same as the yield function and the normality principle is used.

2.6. Data-driven approach for geogrids

The orthotropic model described in the previous sections can be applied to the stress–strain curves obtained from standard tensile tests of geogrids. To successfully implement the model, the following steps are required:

(1) Tensile tests for model calibration: perform uniaxial tensile tests on the geogrid, and obtain the stress–strain curves for a minimum of three directions. The range of directions covered by the orthotropic model will be limited to the directions of the tensile test. Thus, it is common to perform tensile tests between 0 and 90° to better capture the full orthotropic response of the material. Common choices for the uniaxial tensile orientation include 0°, 45° and 90° (Mu et al., 2022), and dividing the direction range into 4 equal parts (0°, 22.5°, 45°, 67.5°, 90°) (Wang et al., 2019).

(2) Evaluate r-values: the stress–strain curves are used to evaluate the r-values using Eq. (13). Initially, a reference stress σ_0 is chosen, and the subsequent ratios are evaluated in relation to the reference stress. The reference stress is taken as the strongest direction. The reference stress can be taken as the yield stress in each direction. Alternatively, for geogrids, the stress at 2 or 5% strain, which are the reference strain values referred in the tensile test standard (ISO-10319, 2015), can be used as reference stresses.

(3) Hill48 parameters estimation: the r-values are used to estimate the Hill48 parameters using the cost function in Eq. (14). For the current study, the Broyden–Fletcher–Goldfarb–Shanno algorithm method is used for optimize the cost function, with an implementation in Python using the SciPy library (Virtanen et al., 2020). It is important to note that the parameters obtained by this optimization are a local minimum and may not guarantee a close match to the entire stress–strain curve spectrum in all directions (Aretz and Barlat, 2013). The yield function is usually well-defined for the range of directions covered by the tensile tests, and when stress–strain curves do not dramatically vary in shape across their main directions, yield accuracy is expected to be good (Hu et al., 2021).

(4) ABAQUS input parameters for the Hill48 model: the anisotropic yield is defined in terms of the stress ratios R_i, and is implemented in ABAQUS by default under the plastic input data, not requiring a user-defined subroutine. The input parameters R_i can be evaluated through the Hill48 parameters obtained int the previous step, using Eq. (18). In ABAQUS, the yield function will be well-defined given that the ratios are positive. For the specific case of plane stress orthotropy, the ratios R_{13} and R_{23} are set to unity, and the remaining ratios are evaluated using the Hill48 parameters.

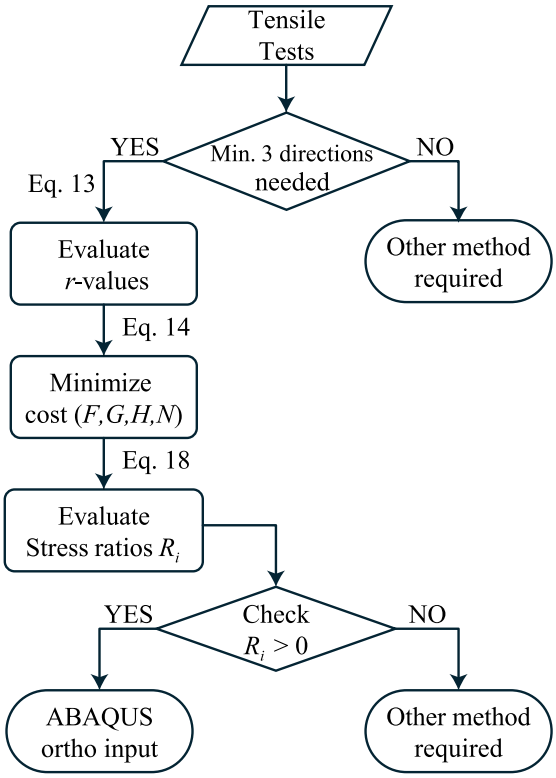

Fig. 2. Procedure to generate orthotropic parameters for ABAQUS.

The Hill48 implementation in ABAQUS requires specification of both the yield surface (through yield ratios) and the hardening behaviour. Isotropic hardening is implemented by defining the yield stress as a function of equivalent plastic strain, extracted from the stress–strain curves obtained in Step 1. The reference yield stress σ_0 and subsequent hardening behaviour are defined through the `*PLASTIC` option (tabular data), while the anisotropic yield ratios are specified through the `*POTENTIAL` option.

This procedure allows for an implementation of the orthotropic model in ABAQUS that can be used in conjunction of both 2D and 3D elements. Given that the plane stress assumption was used to derive the Hill48 parameters, when using 3D elements only normal stresses should be considered. An illustration of the procedure is shown in Fig. 2. While the plane stress assumption is generally valid for thin structures where out-of-plane stresses are negligible, it should be noted that localized stress concentrations at rib junctions may not be captured, as well as contact-induced normal stresses when the geogrid is confined in soil. Moreover, this level of geometric detail is usually not directly included in the 3D model, as the definition of contact interactions between the geogrid and the surround soil would be complex. The reader is referred to (Amirhosseini et al., 2022) on the assessment of the junction thickness in the tensile response, and (Paiva et al., 2023b) on the topology optimization of the junction geometry.

3. Numerical validation

A numerical validation of the proposed procedure is carried out in this section. The previously described procedure will be applied to a geogrid with distinct tensile properties in the main directions, and the orthotropic model is computed using ABAQUS/Standard v2021.

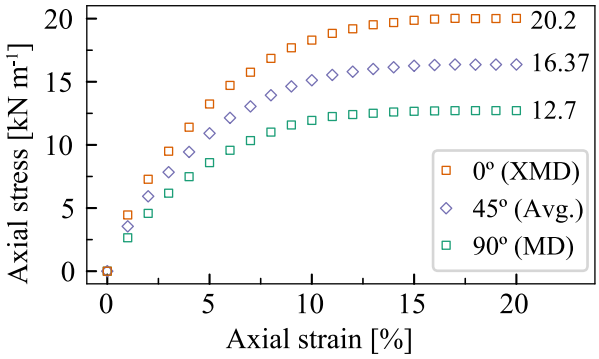

Fig. 3. In-isolation tensile tests in main directions (Hussein and Meguid, 2016).

Table 1
r-values derived for the geogrid tested by Hussein and Meguid (2016).

$r_{0°}$	$r_{45°}$	$r_{90°}$
1	0.8103	0.6287

3.1. In-isolation tensile data

A series of in-isolation tensile tests for a biaxial geogrid was reported by Hussein and Meguid (2016), which were later used in a soil-confined model. The tensile test was carried out according to ASTM (ASTM-D6637-10, 2011) using a 5 kN tensile machine, with a constant strain rate of $10\,\%\,\text{min}^{-1}$. Strains were measured using an extensometer mounted at the centre of the specimen. The reported results of the tensile tests is shown in Fig. 3, where the results from directions of 0° and 90° were tested according to the referred standard, and the results from the 45° direction were obtained by averaging the data from tested directions.

3.2. Constitutive model

The goal of the constitutive model is to describe the orthotropic response of the referred geogrid, capturing the elastic and plastic behaviour of the material. For this, three constitutive components are needed: elastic, plastic and the orthotropic parameters.

The elastic component is defined by the Young's modulus and Poisson's ratio, already estimated by Hussein and Meguid (2016) with values of 605 MPa and 0.3, respectively. Similarly, the plastic components can be obtained from the experimental data, taking special care to convert the engineering stress–strain data into true stress–strain data, the appropriate format for ABAQUS input. Geogrids are known to be highly nonlinear, even at low strains, thus the elastic region is set to be valid until the 1 % strain, with the remaining strain profile taken as plastic. Details of this process are not the focus of this study, and the interested reader is referred to Paiva et al. (2023a) for further information on this procedure.

The orthotropic parameters are evaluated using the procedure described in Section 2.6. The reference stress is taken as the strongest direction (XMD in this case), and for notation consistency, the reference angle for this direction is taken as $\alpha_0 = 0°$. The *r*-values, taken as the ratio between the yield stress in the direction of an angle α and the reference yield stress, are shown in Table 1. The Hill48 parameters are estimated using the cost function in Eq. (14), the results being shown in Table 2. The Hill48 parameters are then converted to the ABAQUS input parameters using Eq. (18), and the results are shown in Table 3.

Table 2
Hill48 parameters derived for the geogrid tested by Hussein and Meguid (2016).

F	G	H	N
1.9683	0.4371	0.5628	1.8427

Table 3
ABAQUS yield ratios for Hill48 model derived for the geogrid tested by Hussein and Meguid (2016).

R_{11}	R_{22}	R_{33}	R_{12}	R_{13}	R_{23}
1	0.6647	0.6653	0.9238	1	1

3.3. Geometry and boundary conditions

The 3D model consists of a rectangular grid with dimensions of $185 \times 58 \times 8\,\text{mm}^3$ with a total of 3 ribs in the longitudinal direction and 6 ribs in the transversal direction. The extruded geogrid featured a junction with a thickness of 2.9 mm and ribs with thickness of 0.8 mm, which was also modelled. The extruding process actually produces a variable rib thickness, but a constant value was used to simplify the model. The full geometric details and simplifications of the 3D model can be found in the original paper by Hussein and Meguid (2016). Each specimen was modelled with 1750 linear brick hexahedral elements with reduced integration (C3D8R), i.e., a single central integration point. This mesh is equivalent of an element size of approximately $2t$, where t is the geogrid rib thickness. The simulation of the tensile test is achieved by restraining the geogrid at the left face (see Fig. 4 case $\alpha = 0°$) and applying a displacement of $10\,\%\,\text{strain}\,\text{min}^{-1}$ at the right face, which for this test is equivalent to a prescribed velocity constraint of $18.5\,\text{mm}\,\text{min}^{-1}$. Sensitivity analysis regarding the mesh, element type and numerical stabilization is not the focus of this study, and the interested reader is referred to Paiva et al. (2023a) for further information on the modelling techniques of geogrids.

When using orthotropic parameters in a FE model, it is necessary to assign a section orientation. This can be done in ABAQUS under the *property* module. Since the model was initially positioned along the global XYZ directions, the section orientation could be easily defined as a simple match and rotation of the global directions. To evaluate the orthotropic model, the same tensile test conditions as the experimental data were applied in three different directions: 0°, 45° and 90°. This allows for an easy visualization and comparison of the directional influence on the tensile response.

3.4. Results of the orthotropic model

The schematics of the three tensile tests, along with the geogrid response in each direction, are illustrated in Fig. 4. In each simulation, the loading and boundary conditions were consistent (in this case, along σ_{11}), with the only variable being the assigned material direction. The results of the orthotropic model are compared against the experimental data from Hussein and Meguid (2016) using the maximum principal stress, $\sigma_{Max,P}$, defined as the maximum stress value among the principal stress directions: $\sigma_{Max,P} = \max\left[\sigma_{11}, \sigma_{22}, \sigma_{33}\right]$. This consistent stress scale across all three directions facilitates a direct comparison of the tensile responses.

Central points (P1, P2, P3) were selected to represent the geogrid response, similar to the approach used in the experimental data collection. The tensile load (y-values) corresponds to the maximum principal stress, and the strain (x-values) corresponds to the maximum principal strain, both evaluated in the same manner. Using maximum principal quantities is a suitable choice for comparisons since the primary objective of uniaxial tensile tests is to evaluate the load–strain response in a specific direction. In such tests, stresses and strains in the remaining directions (e.g., perpendicular direction) are typically lower and often not measured, as they are smaller compared to the principal direction. This approach ensures that the focus remains on the primary directional response, providing a clear representation of the geogrid response and allowing for easy comparison of the orthotropic response.

Good agreement is found between the experimental and simulated tensile tests, with the orthotropic model accurately capturing the directional response of the geogrid in terms of strain and maximum stress. Fig. 4 shows that the full stress limit is only reached when the loading is along the strongest σ_{11} direction (XMD). Because the stress–strain paths are reasonably uniform in terms of format and shape, the orthotropic model was able to accurately replicate the plastic response of the given geogrid.

4. Application to a geogrid-reinforced footing

With the validated orthotropic model, this section addresses the applicability of the proposed 3D modelling framework, the limits where the orthotropic effect can be analysed by this method and how these considerations affect a geosynthetic-reinforced structure response. To this end, a strip footing model, with reported experimental data, will be studied.

4.1. Bearing capacity of geogrid-reinforced soil

Geosynthetics, and geogrids in particular, are widely used to reinforce soil structures. The reinforcement effect is achieved by an increase in the tensile strength of the soil (Koerner, 2012). In such applications, the tensile loads are transferred to the reinforcement through the soil–geogrid interaction. Because of that, the tensile load–strain response of geogrids is a key factor in the design of reinforced soils (Bathurst, 2014).

The bearing capacity of reinforced soil has been studied by many researchers, with both experimental (Xu et al., 2020; Chen et al., 2021; Bhardwaj and Sharma, 2023) and numerical approaches (Thakur et al., 2020; Jamshidi Chenari and Bathurst, 2023; Zhang and Chen, 2023). In these studies, it is clear that geogrids are an effective method to increase the bearing capacity. Moreover, 3D models using finite element techniques can capture many parameters of soil–geogrid structures, such as the stress distribution across reinforcement layers, the interaction properties and the effect of boundary conditions.

Most of the reported numerical models are focused on the overall response of the reinforced structure, usually making use of simplified constitutive models for the geogrids. More complex models, such as the elastic–plastic model proposed by Hussein and Meguid (2016) and the linear-elastic orthotropic model by Zhuang and Wang (2015) have provided great insights into more precise ways to represent geosynthetics response, both in terms of geometry and constitutive laws. The orthotropic model proposed in this study is now evaluated in terms of its applicability to reinforced soil structures, focusing on how the nonlinear orthotropic response can affect the estimates of bearing capacity of the reinforced soil.

4.2. Experimental data of a geogrid-reinforced strip footing

Chen et al. (2009) reported experimental results for a square footing on geogrid-reinforced soil. The parametric tests were devised to evaluate the effect of the number and spacing of layers on the bearing capacity of the reinforced soil. The physical model reported used a box with dimensions of $1500 \times 910 \times 910\,\text{mm}^3$, and a steel plate (representing the strip footing) with dimensions $152 \times 152 \times 25\,\text{mm}^3$ was used to apply a load pressure at the centre of the soil box. The load was applied to constantly maintain a settlement rate of less than $0.03\,\text{mm}\,\text{min}^{-1}$. The box was filled with a crushed limestone, whose properties are summarized in Table 4. A series of parametric tests were performed, with varying numbers of layers and several geosynthetic types. A group of tests were performed with one, two and three layers of the biaxial

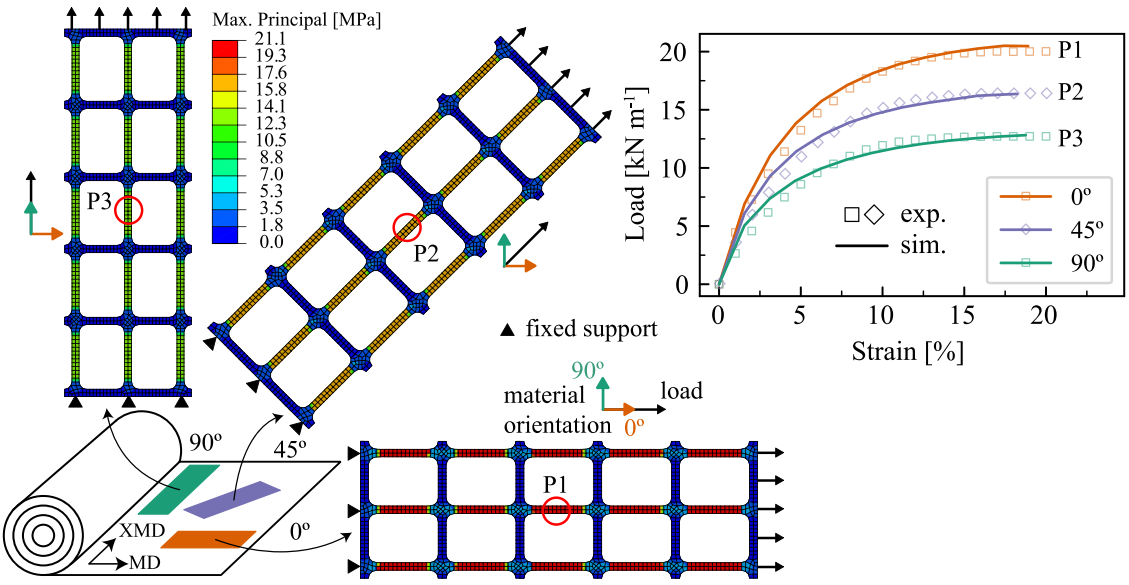

Fig. 4. Stresses and corresponding directions at an angle α with respect to the MD direction (by varying the assigned material direction).

Table 4
Soil properties for the crushed limestone.

Young's Modulus E, [MPa]	Poisson's ratio ν	Friction angle ϕ, [°]	Dilation angle ψ, [°]	Cohesion c, [MPa]
120	0.3	36	21	5×10^{-3} [a]

[a] For numerical stabilization purposes.

geogrid used in the previous section, with a spacing of 500 mm between layers.

4.3. 3D modelling details

ABAQUS/Explicit v2021 package was used to simulate the described experiment, given the high number of contact interactions and the possibility of severe mesh distortion within these contact areas. The 3D geometry was imported in ABAQUS, featuring the soil inside the box and the geogrid layers. The geogrid was modelled using the orthotropic model proposed in this study, with the Hill48 parameters obtained from the in-isolation tensile tests. A geometrical simplification was made, assuming a constant thickness equal to the longitudinal rib, thus not considering the thicker junctions. The implication of this simplification is expected to slightly reduce the bearing capacity (Hussein and Meguid, 2016). The soil was modelled using the Mohr–Coulomb model, with the properties in Table 4. While the Mohr–Coulomb model assumes a linear elastic stress curve and rate-independent behaviour, it provided an adequate representation for the soil bearing capacity analysis under the essentially monotonic loading condition. Full interlocking was assumed between the soil and geogrid, and to that end, three surface-to-surface tie constraint groups were defined: between the lower geogrid face and the bottom soil; between the top geogrid face and the top-soil; and between the geogrid vertical faces and the soil in the apertures. In all tie constraints, the geogrid was allowed to penetrate the soil, this being achieved by setting the geogrid as the slave surface. The soil was modelled with a gradient mesh size of 5 to 50 mm, and the geogrid was modelled with a mesh size of 2 mm. For all materials, and as before, a linear solid brick with reduced integration (C3D8R) were used. The reduced integration formulation was selected for its computational efficiency and to address the complex deformation mechanisms expected in soil–geogrid interaction modelling. Given that the geogrid and the soil in the apertures may experience significant deformation, with possible localized moment concentration, reduced integration elements would compensate the artificial stiffening due to shear locking. Double symmetry was considered, with only a quarter of the model being simulated. The same load pattern as the experimental test was applied to the footing, using a prescribed velocity constraint. To evaluate the bearing capacity, the average of the vertical stress (σ_{33}) acting on the load-area was computed, together with the load-area average vertical settlement (u_{33}). More details of this particular 3D model can be found in the papers by Hussein and Meguid (2016) and Mukherjee and Sivakumar (2023).

4.4. Model validation

The comparison between the predicted settlement and the experimental results is shown in Fig. 5. Three cases were simulated: unreinforced ($N = 0$), one geogrid layer ($N = 1$) and two layers ($N = 2$). Despite its limitations, the Mohr–Coulomb constitutive model was able to reproduce adequately the experimental results for this case study. The model was able to accurately capture the increase in bearing capacity with the addition of geogrid layers, with good agreement with the experimental data. Similarly to what was reported by Hussein and Meguid (2016), the model tends to slightly underpredict the bearing capacity for the reinforced cases, this effect being more pronounced as the settlement increases. For the $N = 2$ case, the model slightly overpredicted the bearing capacity. This was likely due to the complete tie constraint assumption between the geogrid and the soil, which may have led to a more rigid response across all the models in the initial load phase (where there is usually observed some accommodation of the materials), but only showed noticeable impact in the $N = 2$ case.

The $N = 1$ deformed plot for a reference settlement of 14 mm is shown in Fig. 6. Similarly to what is predicted by the experimental tests, the displacements and stresses are concentrated on the loading area (Fig. 6a). A snapshot of the stress distributions in the geogrid is shown in Fig. 6b and Fig. 6c, where the orthotropic model was able to capture the stress nuances across the main directions. Even though the geogrid is considerably stiffer in the XMD direction, the actual soil–geogrid stress response was relatively similar across the XMD and MD directions, likely due to the symmetry of the strip footing and loading conditions.

Since geogrids are designed to be used in conjunction with soil, the next section uses this validated model to evaluate the influence of orthotropy in the soil–geogrid response.

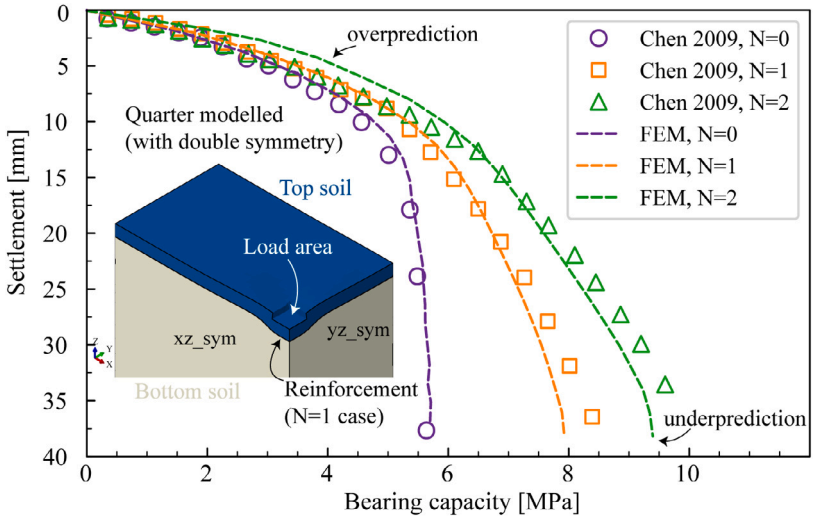

Fig. 5. Load-settlement for geogrid-reinforced strip footing — experimental and numerical results.

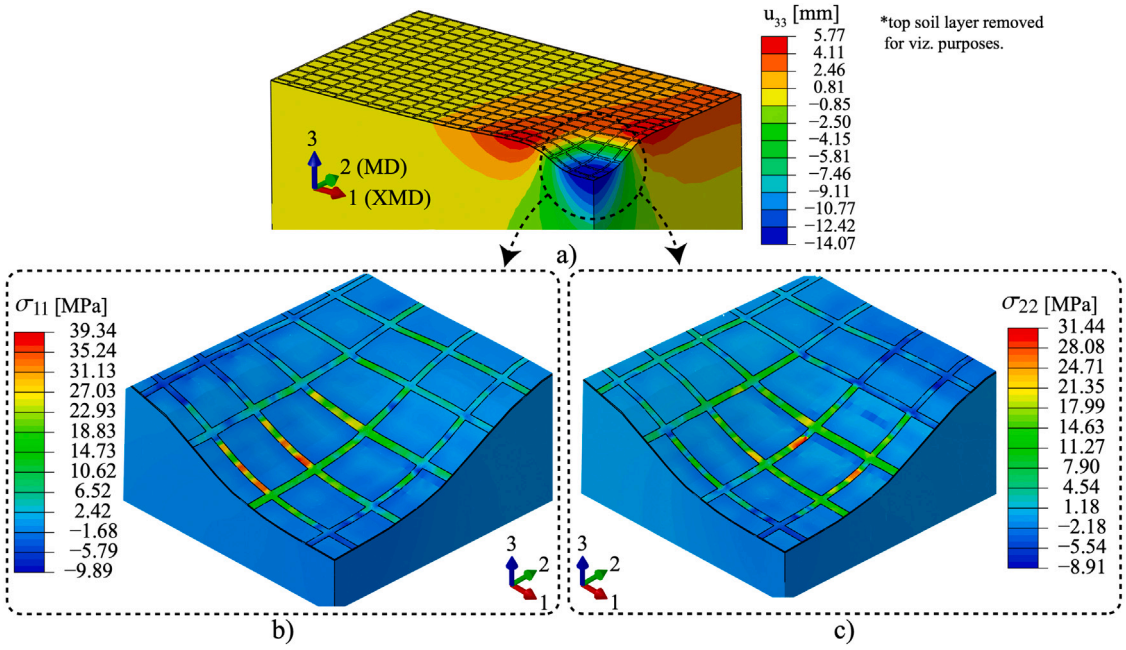

Fig. 6. Displacements and stresses for a reference settlement of 14 mm with one reinforcement layer: (a) Vertical displacements (u_{33}); (b) Stress along the XMD direction (σ_{11}); (b) Stress along the MD direction (σ_{22}).

4.5. Influence of orthotropy in the soil-reinforcement response

In this section, two groups of numerical tests are performed to evaluate the orthotropy effect: the first test group evaluates the effect of the orthotropy level, and the second test group evaluates the effect of notches (bar cuts) in the stress redistribution within the geogrid.

4.5.1. Orthotropy testing scenarios

Orthotropy level. To evaluate the effect of material orthotropy in the soil–geogrid response, a parametric study was carried out with three different orthotropy levels. A theoretical geogrid with average maximum stress of 50 MPa at 20 % strain was used. An orthotropy index ξ, defined as the ratio between the maximum stress in the XMD direction and the MD direction, $\xi = \sigma_{XMD}/\sigma_{MD}$, was varied in such way that the average stress remained constant and equal to 50 MPa in all cases. The summary of maximum tensile stresses, together with the Young's modulus estimation for each case is presented in Table 5. A similar load–strain pattern to that of the previous tests was used, with the three test cases shown in Fig. 7.

Table 5
Tensile properties for orthotropy parametric test.

Case study	E [MPa]	σ_{xmd} [MPa]	σ_{md} [MPa]	ξ_{12} [–]
Case I	1000	50	50	1
Case II	1300	62	38	1.6
Case III	1800	76	24	3.2

The three test cases were fetched to the previously validated 3D model described in Section 4.3, altering solely the tensile properties of the geogrid, and the bearing capacity was evaluated for each case.

Notches. To evaluate the effect of orthotropy on the redistribution of stresses in the case of bar cuts, a batch of cuts was made in the geogrid,

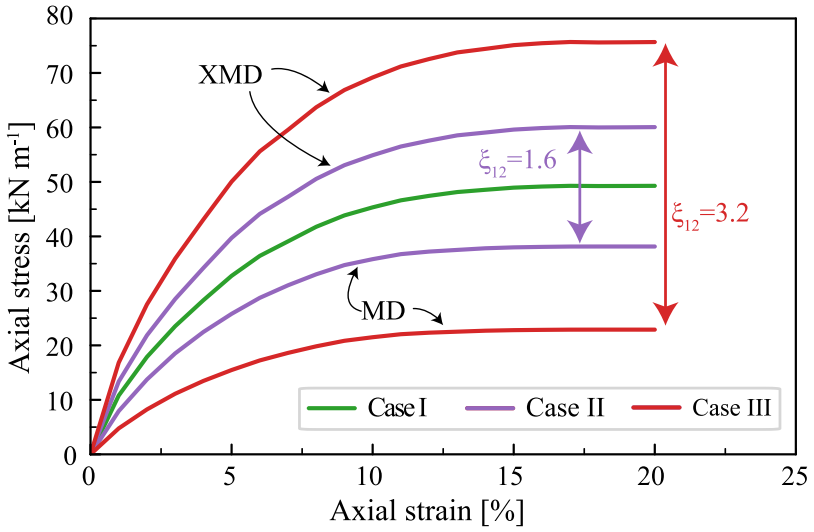

Fig. 7. Stress–strain response in XMD and MD for the three orthotropy levels studied.

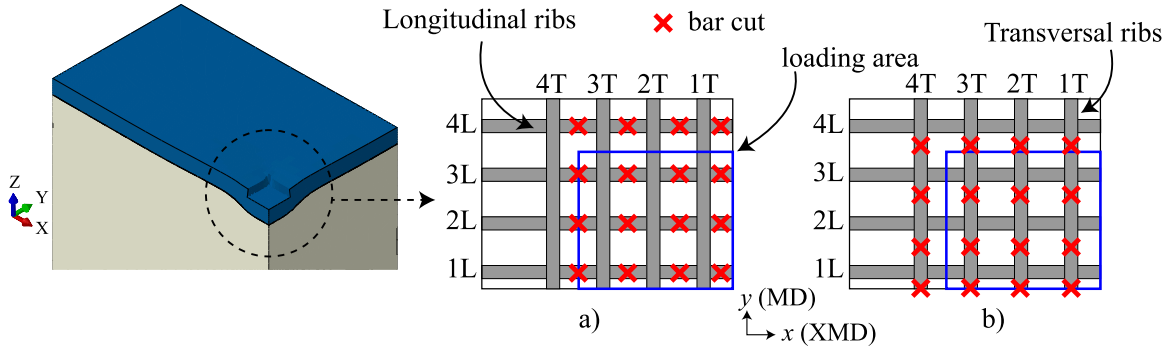

Fig. 8. Notches test setup on loading area: (a) Cuts on the longitudinal ribs; (b) Cuts on the transversal ribs.

as shown in Fig. 8. In total, 16 cuts were made in the geogrid for each test case, those being on the first 4 longitudinal bars (starting from where the load was applied), and Similarly to the first 4 transversal bars. Since the interaction between the soil and the geogrid was taken as fully interlocked, the notches were, in fact, achieved by removing the referred bar segments from the geogrid. The remaining testing conditions were kept the same as the previously validated tests, and the stresses in the most critical zone (near the end of the loading area) were evaluated for each case.

4.5.2. Orthotropy level results

The results of the orthotropy impact in the load-settlement are shown in Fig. 9. The average (isometric, case I) assumption tends to preserve the curve format, being a reasonable approximation for low levels of orthotropy. With increasing orthotropy, the bearing capacity is increased for the same relative settlement, being particularly pronounced in higher strain levels (for settlement larger than 10 mm). The cumulative increase in bearing capacity, with respect to the average isotropic assumption, is shown in Fig. 9b. This was obtained by the mean difference of bearing capacity results across the domain (0 to 40 mm in this case). The progression shows an exponential tendency for the isotropic model to underpredict the bearing capacity of the given strip footing.

It is worth mentioning that the increase in bearing capacity and the respective cumulative difference is likely due to a combination of factors, such as the increased stiffness in the XMD direction, and also the required increase in the Young's modulus (for the orthotropic case) to correctly match the average stress response. That is, the isotropic assumption also requires an average value for the Young's modulus, which can be an underprediction for the stronger direction or an overprediction for the weaker direction in a highly orthotropic material. To test this hypothesis, the Young's modulus was increased in the isotropic model to match that of the XMD direction in the orthotropic model of case III. The regular isotropic, the corrected isotropic and the reference orthotropic models are shown in Fig. 10, where a better match is observed between the corrected isotropic and the orthotropic reference.

A final remark on the orthotropic index is that, for values of ξ higher than 3.2 (case III), the presented orthotropic model was no longer well-defined, with negative yield ratios. For stress–strain responses of geogrids, namely the type A response referred by Liu and Ling (2006), a higher level of orthotropy may require a different yield function.

4.5.3. Notches results

The results for the stress distributions, for a reference settlement of 25 mm in the loading area with the addition of notches are shown in Fig. 11. Noticeable higher stresses are observed in the geogrid of the orthotropic cases, indicating that the reinforcement is mobilizing more of its strength. This suggests that the orthotropic model allows for a more effective redistribution of stresses in the presence of notches. Moreover, the higher negative stresses (indicating compression in this

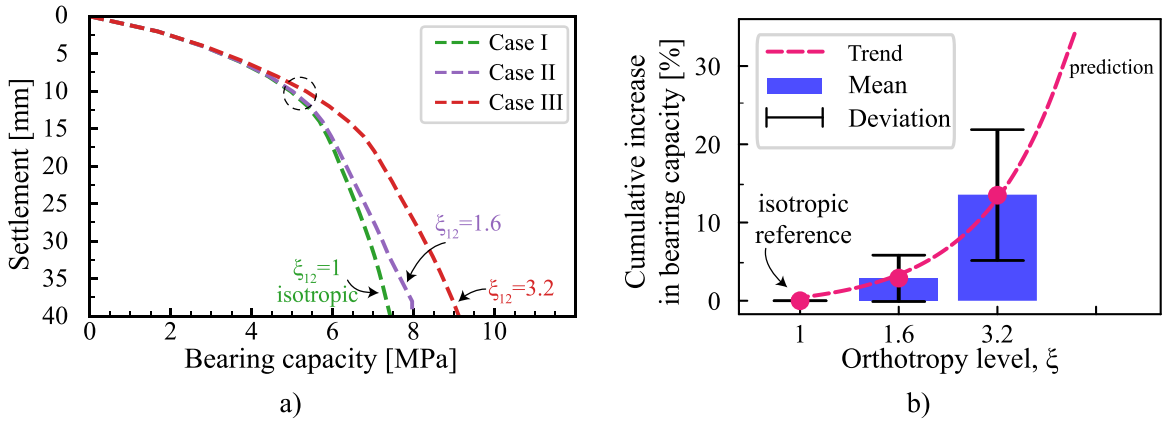

Fig. 9. Effect of orthotropy level on the bearing capacity: (a) Load-settlement plot; (b) Cumulative difference with relation to the isotropic assumption.

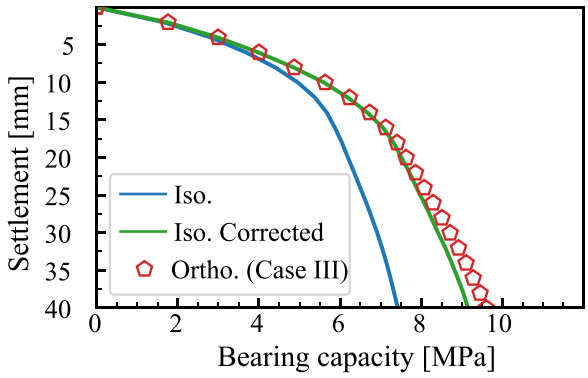

Fig. 10. Load-settlement plot and influence of isotropic model with calibrated Young's modulus.

case) in the soil closer to the geogrid for the σ_{11} also indicates that the orthotropic model is able to better capture the reinforcement effect of the geogrid in the soil.

4.6. Limitations and areas of improvement

This study on the 3D orthotropic response of geogrids presents some hypotheses that should be considered:

- the orthotropic equations were derived under the assumption of plane stress conditions, which is a common assumption for most geogrids used in the function of reinforcement. In case of more complex grid geometries or specific stress conditions, a more comprehensive stress analysis might be required.
- the estimation of the orthotropic response was performed using standard short-term tensile test data and a cost function optimization. While this method provides a good approximation for the tensile response, it may not capture all nuances of more complex responses such as creep or cyclic loading. Moreover, the stress–strain curve format (see Liu and Ling (2006)) could not be optimized under high levels of orthotropy, which may require a different yield function.
- The orthotropic model was calibrated using data obtained from tensile tests (carried out at a loading rate of 18.5 mm min^{-1}). This can be relatively high for a real-life application. Nevertheless, the calibration exercised performed showed good agreement with experimental data obtained for loading rate of the footing of the overall model of 0.03 mm min^{-1} at the surface.

5. Summary and conclusions

This study detailed a simple 3D orthotropic modelling framework for the short-term tensile response of geogrids using the Hill48 yield criterion. The proposed data-driven approach enables the calibration of orthotropic parameters directly from standard tensile test data, making it readily implementable in commercial finite element software like ABAQUS without requiring complex user-defined subroutines. The model was validated through in-isolation tensile tests and applied to a realistic geogrid-reinforced strip footing problem to evaluate the influence of material orthotropy on both reinforcement behaviour and overall structural response compared to traditional isotropic assumptions. Based on the numerical analyses of the discussed 3D orthotropic framework, several conclusions can be drawn:

- The orthotropic Hill48 model, combined with standard short-term tensile test data, provides a feasible and straightforward approach to capture the anisotropic tensile response of geogrids. The model showed good agreement with experimental data and can be implemented directly in ABAQUS without the need for complex user-defined subroutines. The Hill48 model is also built-in in many other popular FEM packages used in engineering.
- The orthotropic model was able to predict the bearing capacity of geogrid-reinforced soil with good accuracy. The results indicated that the orthotropic properties of geogrids could lead to improved reinforcement performance (in the order of 20% for the reported strip footing model) when compared to the traditional isotropic assumption, particularly under higher orthotropic levels.
- In the presence of notches, the orthotropic model demonstrated a higher capability to redistribute stresses within the geogrid and the soil–geogrid interface (between 10% and 20% for the reported strip footing model). This suggests that the model can effectively capture the stabilization mechanisms in reinforced structures.
- The study highlighted the importance of accurately determining the orthotropic parameters and the Young's modulus for different directions. Simplified isotropic assumptions can lead to underprediction or overprediction of the reinforcement effect, particularly for highly orthotropic materials.

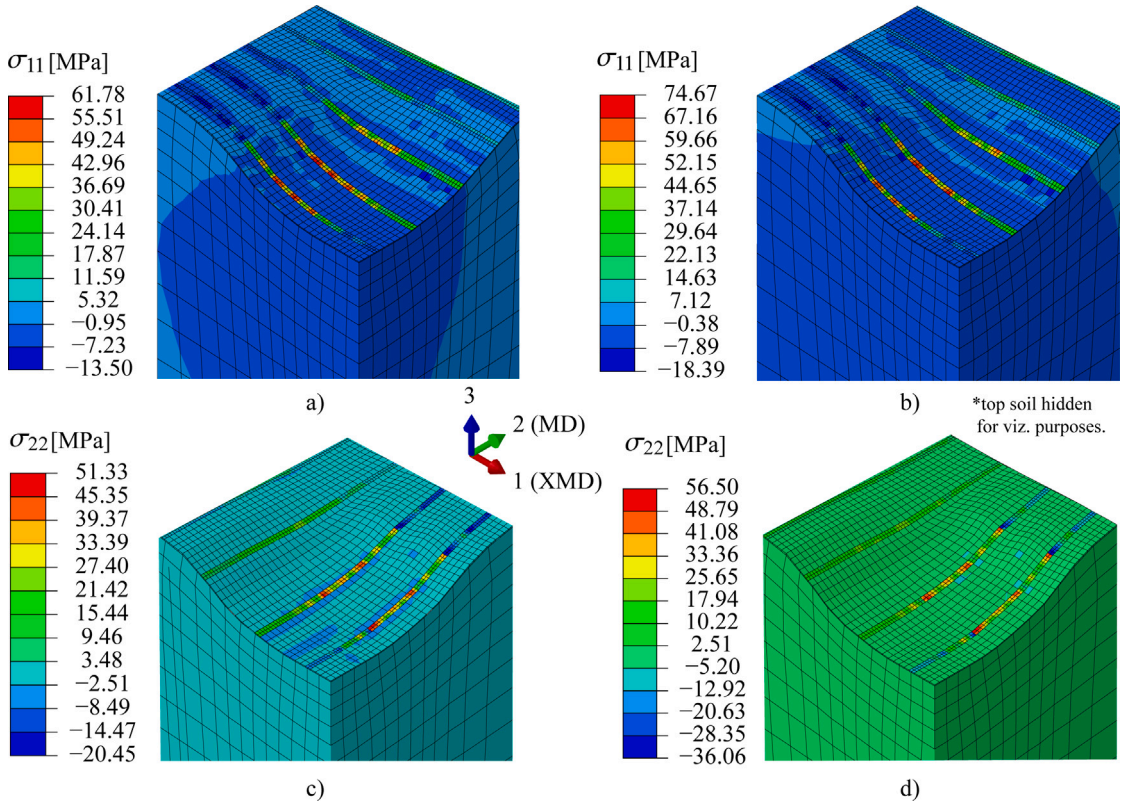

Fig. 11. Stress distribution for a reference settlement of 25 mm: (a) Isotropic Notches MD; (b) Orthotropic Notches MD; (c) Isotropic Notches XMD; (d) Orthotropic Notches XMD.

CRediT authorship contribution statement

Lucas Paiva: Writing – original draft, Methodology, Formal analysis, Data curation, Conceptualization. **Margarida Pinho-Lopes:** Writing – review & editing, Validation, Supervision, Project administration, Conceptualization. **Robertt Valente:** Writing – review & editing, Validation, Supervision, Project administration, Conceptualization. **António Miguel Paula:** Writing – review & editing, Validation, Supervision, Project administration, Conceptualization.

Declaration of competing interest

The authors declare that they have no known competing financial interests or personal relationships that could have appeared to influence the work reported in this paper.

Acknowledgements

The first author acknowledges the financial support by the Portuguese Foundation of Science and Technology – FCT under the MIT Portugal PhD Grant PRT/BD/153383/2021. The financial support of FCT is also gratefully acknowledged through the projects UIDB/04625/2025 (CERIS), UIDB/00481/2020 (TEMA), UIDP/04450/2020 and CENTRO-01-0145-FEDER-022083 (CENTRO 2020). This study was funded by the PRR—Recovery and Resilience Plan and by the NextGenerationEU funds at Universidade de Aveiro, through the scope of the Agenda for Business Innovation "Transform - Transformação digital do setor florestal para uma economia resiliente e hipocarbónica" (Project no.34 with the application C644865735-00000007).

Data availability

The Hill48 python script and the ABAQUS files can be found in https://github.com/luccpaiva/ortho-model.

References

Abaqus, 2021. ABAQUS/Standard User's Manual, Version 2021. Dassault Systèmes Simulia Corp.

Akter, S.T., Serrano, E., Bader, T.K., 2021. Numerical modelling of wood under combined loading of compression perpendicular to the grain and rolling shear. Eng. Struct. 244, 112800. http://dx.doi.org/10.1016/j.engstruct.2021.112800.

Al-Barqawi, M., Aqel, R., Wayne, M., Titi, H., Elhajjar, R., 2021. Polymer geogrids: A review of material, design and structure relationships. Materials 14, 4745. http://dx.doi.org/10.3390/ma14164745.

Amirhosseini, I., Toufigh, V., Toufigh, M.M., Ghazavi-Baghini, E., 2022. Three-dimensional modeling of geogrid pullout test using finite-element method. Int. J. Geomech. 22, 04021297. http://dx.doi.org/10.1061/(ASCE)GM.1943-5622.0002218.

Aretz, H., Barlat, F., 2013. New convex yield functions for orthotropic metal plasticity. Int. J. Non-Linear Mech. 51, 97–111. http://dx.doi.org/10.1016/j.ijnonlinmec.2012.12.007.

ASTM-D6637-10, 2011. Standard test method for determining tensile properties of geogrids by the single or Multi-Rib Tensile method. Standard.

Barlat, F., Lege, D.J., Brem, J.C., 1991. A six-component yield function for anisotropic materials. Int. J. Plast. 7, 693–712. http://dx.doi.org/10.1016/0749-6419(91)90052-z.

Bathurst, R.J., 2014. Challenges and recent progress in the analysis, design and modelling of geosynthetic reinforced soil walls. In: Proceedings of the 10th International Conference on Geosynthetics-Giroud Lecture, vol. 21–25, p. 38, 2014.

Bhardwaj, A., Sharma, R.K., 2023. Experimental and numerical investigations on the bearing capacity of footings on the layered soil. Int. J. Geosynth. Ground Eng. 9, http://dx.doi.org/10.1007/s40891-023-00461-y.

Bruschi, S., Altan, T., Banabic, D., Bariani, P., Brosius, A., Cao, J., Ghiotti, A., Khraisheh, M., Merklein, M., Tekkaya, A., 2014. Testing and modelling of material behaviour and formability in sheet metal forming. CIRP Ann 63, 727–749. http://dx.doi.org/10.1016/j.cirp.2014.05.005.

Cardoso, R., Adetoro, O., 2018. Generalisation of hill's yield function for planar plastic anisotropy. J. Phys.: Conf. Ser. 1063, 012112. http://dx.doi.org/10.1088/1742-6596/1063/1/012112.

Chen, Q., Abu-Farsakh, M., Sharma, R., 2009. Experimental and analytical studies of reinforced crushed limestone. Geotext. Geomembranes 27, 357–367. http://dx.doi.org/10.1016/j.geotexmem.2009.03.002.

Chen, J., Guo, X., Sun, R., Rajesh, S., Jiang, S., Xue, J., 2021. Physical and numerical modelling of strip footing on geogrid reinforced transparent sand. Geotext. Geomembranes 49, 399–412. http://dx.doi.org/10.1016/j.geotexmem.2020.10.011.

Dunne, F., Petrinic, N., 2005. Introduction To Computational Plasticity. OUP Oxford.
Ezzein, F.M., Bathurst, R.J., Kongkitkul, W., 2015. Nonlinear load–strain modeling of polypropylene geogrids during constant rate-of-strain loading. Polym. Eng. Sci. 55, 1617–1627.
Gajewski, M., Jemioło, S., 2014. Orthotropic composite constitutive model of mineral–asphalt mix reinforced with grid and its approximation with an isotropic model. Road Mater. Pavement Des. 15, 521–538. http://dx.doi.org/10.1080/14680629.2014.884977.
Haddadi, H., Bouvier, S., Banu, M., Maier, C., Teodosiu, C., 2006. Towards an accurate description of the anisotropic behaviour of sheet metals under large plastic deformations: Modelling, numerical analysis and identification. Int. J. Plast. 22, 2226–2271. http://dx.doi.org/10.1016/j.ijplas.2006.03.010.
Hill, R., 1948. A theory of the yielding and plastic flow of anisotropic metals.. Proceedings of the Royal Society of London. Series A.Math. Phys. Sci. 193, 281–297. http://dx.doi.org/10.1098/rspa.1948.0045.
Hill, R., 1958. A general theory of uniqueness and stability in elastic–plastic solids. J. Mech. Phys. Solids 6, 236–249. http://dx.doi.org/10.1016/0022-5096(58)90029-2.
Hill, R., 1993. A user-friendly theory of orthotropic plasticity in sheet metals. Int. J. Mech. Sci. 35, 19–25. http://dx.doi.org/10.1016/0020-7403(93)90061-x.
Hu, Q., Yoon, J.W., Manopulo, N., Hora, P., 2021. A coupled yield criterion for anisotropic hardening with analytical description under associated flow rule: Modeling and validation. Int. J. Plast. 136, 102882. http://dx.doi.org/10.1016/j.ijplas.2020.102882.
Huang, Z., Ziotopoulou, K., Filz, G.M., 2020. 3D numerical analyses of column-supported embankments: Failure heights, failure modes, and deformations. J. Geotech. Geoenvironmental Eng. 146, http://dx.doi.org/10.1061/(asce)gt.1943-5606.0002385.
Hussein, M., Meguid, M., 2016. A three-dimensional finite element approach for modeling biaxial geogrid with application to geogrid-reinforced soils. Geotext. Geomembranes 44, 295–307. http://dx.doi.org/10.1016/j.geotexmem.2015.12.004.
ISO-10319, 2015. BS EN ISO 10319:2015: Geosynthetics – wide-width tensile test. Standard.
Jamshidi Chenari, R., Bathurst, R.J., 2023. Influence of geosynthetic stiffness on bearing capacity of strip footings seated on thin reinforced granular layers over undrained soft clay. Geotext. Geomembranes 51, 43–55. http://dx.doi.org/10.1016/j.geotexmem.2022.09.006.
Khalfallah, A., Alves, J.L., Oliveira, M.C., Menezes, L.F., 2015. Influence of the characteristics of the experimental data set used to identify anisotropy parameters. Simul. Model. Pr. Theory 53, 15–44. http://dx.doi.org/10.1016/j.simpat.2015.02.007.
Koerner, R.M., 2012. Sixth ed. Designing with Geosynthetics, vol. 1, Xlibris Corporation.
Lian, J., Shen, F., Jia, X., Ahn, D.C., Chae, D.C., Münstermann, S., Bleck, W., 2018. An evolving non-associated hill48 plasticity model accounting for anisotropic hardening and r-value evolution and its application to forming limit prediction. Int. J. Solids Struct. 151, 20–44. http://dx.doi.org/10.1016/j.ijsolstr.2017.04.007.
Liu, H., Ling, H., 2006. Modeling cyclic behavior of geosynthetics using mathematical functions combined with masing rule and bounding surface plasticity. Geosynth. Int. 13, 234–245. http://dx.doi.org/10.1680/gein.2006.13.6.234.
Mu, Z., Zhao, J., Meng, Q., Zhang, Y., Yu, G., 2022. Limitation analysis of the hill48 yield model and establishment of its modified model for planar plastic anisotropy. J. Mater. Process. Technol. 299, 117380. http://dx.doi.org/10.1016/j.jmatprotec.2021.117380.
Mukherjee, S., Sivakumar, B.G., 2023. Three-dimensional numerical modeling of geogrid reinforced foundations. Comput. Geotech. 158, 105397. http://dx.doi.org/10.1016/j.compgeo.2023.105397.
Neto, D., Oliveira, M., Alves, J., Menezes, L., 2014. Influence of the plastic anisotropy modelling in the reverse deep drawing process simulation. Mater. Des. 60, 368–379. http://dx.doi.org/10.1016/j.matdes.2014.04.008.
Paiva, L., Pinho-Lopes, M., Valente, R., Paula, A.M., 2023a. Three-dimensional modelling of in-isolation tensile response of geogrids using hyperbolic constitutive models. Finite Elem. Anal. Des. 225, 104008. http://dx.doi.org/10.1016/j.finel.2023.104008.
Paiva, L., Pinho-Lopes, M., Valente, R., Paula, A.M., 2023b. Topology Optimization of a Junction in a Biaxial Geogrid under in-Isolation Tensile Loading. CRC Press, pp. 2140–2145. http://dx.doi.org/10.1201/9781003386889-288, (Chapter 1).
Perkins, S., 2000. Constitutive modeling of geosynthetics. Geotext. Geomembranes 18, 273–292. http://dx.doi.org/10.1016/S0266-1144(99)00021-7.
Shukla, S.K., 2006. An Introduction To Geosynthetic Engineering, first ed. Taylor & Francis.
Thakur, A., Rawat, S., Gupta, A.K., 2020. Experimental and numerical modelling of group of geosynthetic-encased stone columns. Innov. Infrastruct. Solutions 6, http://dx.doi.org/10.1007/s41062-020-00379-8.
Virtanen, P., Gommers, R., Oliphant, T.E., Haberland, M., Reddy, T., Cournapeau, D., Burovski, E., Peterson, P., Weckesser, W., Bright, J., et al., 2020. Scipy 1.0: fundamental algorithms for scientific computing in python. Nature Methods 17, 261–272. http://dx.doi.org/10.1038/s41592-019-0686-2.
Wang, H., Men, M., Yan, Y., Wan, M., Li, Q., 2019. Prediction of eight earings in deep drawing of 5754o aluminum alloy sheet. Chin. J. Mech. Eng. 32, http://dx.doi.org/10.1186/s10033-019-0390-2.
Wang, H., Wan, M., Wu, X., Yan, Y., 2009. The equivalent plastic strain-dependent yld2000-2d yield function and the experimental verification. Comput. Mater. Sci. 47, 12–22. http://dx.doi.org/10.1016/j.commatsci.2009.06.008.
Wu, H.C, 2002. Anisotropic plasticity for sheet metals using the concept of combined isotropic-kinematic hardening. Int. J. Plast. 18, 1661–1682. http://dx.doi.org/10.1016/s0749-6419(01)00060-2.
Xu, Y., Yan, G., Williams, D.J., Serati, M., Scheuermann, A., Vangsness, T., 2020. Experimental and numerical studies of a strip footing on geosynthetic-reinforced sand. Int. J. Phys. Model. Geotech. 20, 267–280. http://dx.doi.org/10.1680/jphmg.18.00021.
Zhang, W., Chen, 2023. Numerical modeling of geosynthetic reinforced soil retaining walls with different toe restraint conditions. Geotext. Geomembranes 51, 16–29. http://dx.doi.org/10.1016/j.geotexmem.2022.09.002.
Zhang, M., Javadi, A., Lai, Y., Sun, J., 2006. Analysis of geosynthetic reinforced soil structures with orthogonal anisotropy. Geotech. Geol. Eng. 24, 903–917. http://dx.doi.org/10.1007/s10706-005-7722-y.
Zhu, J., Xia, Y., Luo, H., Gu, G., Zhou, Q., 2014. Influence of flow rule and calibration approach on plasticity characterization of dp780 steel sheets using hill48 model. Int. J. Mech. Sci. 89, 148–157. http://dx.doi.org/10.1016/j.ijmecsci.2014.09.001.
Zhuang, Y., Wang, K., 2015. Three-dimensional behavior of biaxial geogrid in a piled embankment: numerical investigation. Can. Geotech. J. 52, 1629–1635. http://dx.doi.org/10.1139/cgj-2014-0538.